Crack propagation in grooved long bone segment

Théophile Kurtz, Y Godio-Raboutet, J.-L Tailhan

Crack propagation in grooved long bone segment

T. KURTZ[a]*, Y. GODIO-RABOUTET[a], J.-L. TAILHAN[b]

a. Aix Marseille Univ, Univ Gustave Eiffel, LBA, Marseille, France
*theophile.kurtz@univ-eiffel.fr / yves.godio-raboutet@univ-eiffel.fr
b. Université Gustave Eiffel, MAST-EMGCU, Marne la Vallée, France
jean-louis.tailhan@univ-eiffel.fr

Translation note

The following paper is an english translation of the scientific article "T. Kurtz, Y. Godio-Raboutet, and J.-L. Tailhan. Propagation de fissure sur tronçon d'os long rainuré. 25ème congrès français de mécanique, nantes, france. 2022." [1]. The original version is published in french along the work presented during the 25th French Congress of Mechanics in Nantes (from August 29th to September 2nd of 2022).

URL link to the original article : https://hal.science/hal-04280203v1

Abstract

A mechanical test of macrocrack propagation in a cortical bone shaft is developed to comprehend the failure mechanisms at this scale and identify fracture processes, which are paramount to a future modelisation. A first set of three-point bending tests was performed on notched segments of human femoral dyaphisis [2, 3]. However, macrocrack orientation is influenced by the material's anisotropy. In order to drive cracking processes in the transversal direction only, a modification of the testing protocol is submitted.

From work found in the litterature [4, 5], notched shafts are previously grooved : a hemispherical groove is milled on the external surface of the bone to guide the crack in the transversal direction in the notch section. Special care is taken for the three-point bending test allowing a mastered procedure despite geometric variability of specimens : positioning and boundary conditions of the samples, notch displacement sensor's supports alignment regarding bone axis, positioning and height of the notch, constant groove's depth. The hydraulic jack is driven indirectly with the notch opening, measured with an inductive displacement sensor. A series of unloading/reloading cycles are done to plot residual quantities, pre-peak damage and macrocrack propagation in post-peak.

Obtained results are expressed in terms of loading as a function of the notch opening displacement. Load-unloading cycles and residual openings analysis highlight the prominent role of cracking in failure mechanisms. Results show that the residual opening is directly linked to a structural weakening, consequently to the cracking processes, and that no plasticity is found at this scale. Cycles analysis allows us to develop a hypothesis about the role of internal residual stresses on permanent deformation. Furthermore, results point out that the groove guides the macrocrack in the transversal direction. Comparison between results on non-grooved samples exhibits the impact of the geometric feature. Future perspectives rely on the reverse analysis determination of the mechanical properties in the transversal direction.

Keywords : Mechanical test, Crack propagation, Three-point bending, Cortical bone

1 Introduction

The skeleton is the framework that ensures the physical integrity of the human body. It is subjected to different loads during the daily life and can fracture. This quasi-fragile biological tissue has a hierarchical and multi-scale internal structure, as well as a high degree of heterogeneity. It is also characterized by a significant variability between subjects [6] and within subjects. The study of fracture properties, particularly through tests on the initiation and propagation of cracks in human bone tissue, represents a vast area of study within the field of biomechanics. These tests serve, on one hand, to illustrate and understand the physical mechanisms [7, 8, 9, 10, 11], and on the other hand, to determine mechanical properties such as strength and toughness [7, 12, 13, 14, 15, 16]. These data are essential for the development of cracking models. However, the majority of them are conducted on machined specimens with controlled and small dimensions, thus not taking into account the unique morphology of the bone.

The test presented, whose initial developments were published in [3], focuses on the study of the propagation of a macrocrack in a section of a long human bone segment. Working at this scale has the advantage of not requiring specific tooling for specimen fabrication and simplifying their realization. However, the major drawbacks include: (i) the control of the boundary conditions of a specimen with irregular geometry and (ii) the post-processing of results for the determination of mechanical parameters with the 3D reconstruction of a biofidelic numerical model of the test.

The test involves a three-point bending on a bone segment, pre-notched at mid-span. Fine control of crack propagation is ensured by indirect control of the press cylinder using the measurement of the notch opening. Furthermore, a modification to the original test [3] is proposed to maintain a transverse propagation of the macrocrack. To achieve this, it is necessary to modify the stress field with two possible choices: either orthoradially prestrain[1] the specimen or locally reduce its central section. The latter option was chosen for its technical simplicity, involving machining a hemispherical groove around the outer surface of the bone in the notch section. Simultaneously, significant improvements in the reproducibility and repeatability of the test have also been made. The primary goal of interpreting the obtained results is to better understand the physical mechanisms involved in the transverse fracture of bone.

2 Materials and methods

2.1 Sampling and preservation

The femurs are harvested from Post-Mortem Human Subjects (PMHS), initially embalmed by injecting a solution of zinc chloride, except for specimen 150-17D, embalmed with formaldehyde. Tissue manipulations are carried out under the ethical supervision of the Faculty of Medicine of Marseille. Data related to the subjects are summarized in table 1.

The tissues are cleaned and degreased manually, removing connective tissues with hot water, without the use of chemicals. The femoral bone is then cut in the diaphysis to obtain a 180 mm section. For

[1] In compression.

the sake of simplification, the study focuses on cortical tissue (future work will focus on the fracture behavior of trabecular bone). Trabecular bone and marrow are manually removed by scraping.

The bones are stored in a freezer at a controlled temperature of -18°C. On the day before a test, the specimen is stored in a refrigerator at 4°C. The preparation, instrumentation, and adjustment phases are carried out at room temperature (20°C). After the test, the broken specimen is once again stored at -18°C.

Table 1: Subject's references: Age (years), Sex (F for female, M for male), Laterality (femur of origin, left (G) or right (D)

Subject	Age (years)	Sex	Laterality
150-17D	83	F	Right
61-21G	82	M	Left
90-21D	70	M	Right
43-20G	73	M	Left
80-21D	86	M	Right

2.2 Preparation of a sample

On the day of the test, the specimen, which has been thawed the day before, is positioned on the test rig. To ensure reproducibility of the test, each bone is tested in the same orientation relative to common anatomical features. The load is applied on the rough line (linea aspera) of the femoral section, at the level of the central cross-sectional area. The anterior face of the bone is oriented towards the supports. This sample position is chosen because it is naturally the most stable.

Due to the irregular and variable geometry of the samples, small parallelepipedic metal prisms (7mm x 5mm x 20mm) are bonded with cyanoacrylate adhesive to locally distribute the stresses to the supports and prevent tilting of the specimen. The bonding is carried out under the press directly, with a load of 30 N, to ensure they remain tangent to the anterior face of the bone. Their positioning and longitudinal alignment are ensured by a 3D-printed guide with reference to the loading head. To avoid any detrimental friction at the supports and ensure proper functioning in simple bending of the bone, it should be noted that one of the prisms is designed to be "sliding." It is actually composed of two half-blocks (sliding relative to each other). The contact surfaces of the two half-blocks are machined, polished, and lubricated[2]. The assembly is held in place by an elastic membrane, which also ensures elastic return to the initial position during unloading of the specimen.

Once the supports are glued, a notch with a thickness of $200\,\mu\mathrm{m}$ is machined in the central section of the bone using a scroll saw. The bone is positioned on a carriage guided on the saw table. Its position on this carriage is adjusted using a 3D-printed piece simulating, identically, the positions of the press supports and the loading head. A 7.5 mm slip gauge is used to set the stops of the carriage on the saw table and fix the depth of the notch machining.

To guide the macrocrack in the transverse direction, a semi-circular section groove is milled around the external surface at the notch section. It is crucial to ensure a constant depth of 2 mm. The tool used is a tungsten carbide spherical cutter, Dremel 225. A 3D-printed cap is screwed onto the manual support of the cutter and slightly protrudes. The depth is calibrated with a 2 mm standard shim. The particularity of the cap is its semi-spherical shape, ensuring a constant machining depth on the bone despite the irregular

[2] With lithium grease.

geometry of its external surface. This step is carried out under a water jet to avoid necrosing the bone tissue and risking excessive alteration of its properties.

The sensor measuring the notch opening must be attached to aluminum supports bonded to the bone. A new guide, also 3D-printed, holds these sensor supports in the bonding position and adjusts their alignment with respect to the metal supports. A point of cyanoacrylate adhesive is deposited on the surface of the supports. The anterior face of the bone section is then placed on the guide so that the supports are positioned on either side of the notch and aligned with the supports. This crucial step ensures proper positioning of the assembly for all tests.

Once all these steps are completed, the specimen is finally positioned on the test rig.

2.3 Mechanical test

The three-point bending mechanical test is conducted on an MTS Landmark 370.10 hydraulic press equipped with a 15 kN force sensor. The span between the supports of the press is 155 mm. A KAMAN KD-2300 inductive displacement sensor, with a measurement range of 0-2 mm, measures the Notch Opening Displacement (NOD). This sensor measures the relative distance between its support and a target glued to the opposing support. Both supports are made of aluminum to avoid creating electromagnetic disturbances that could affect the measurement. Figure 1 shows the test setup.

The quantities measured during the test are:

- The applied load in N
- The NOD in mm

The experimental procedure follows the steps defined in [3]. It involves loading the specimen at its center and applying ten cycles of unloading-reloading during the test. The loading is driven via the notch opening at a speed of $36\,\mu\mathrm{m/min}$, considered quasi-static. The effects of loading speed are not evaluated in this study and should be part of a separate investigation. The cycles step is $200\,\mu\mathrm{m}$ from 0 up to 2 mm. The unloading is force-driven to reach 15 N within 5 minutes.

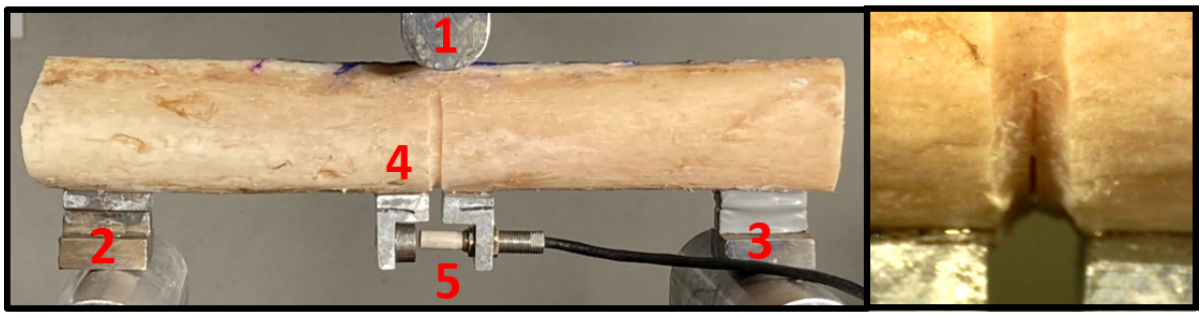

Figure 1: Three-point bending test with indirect control by notch opening. 1) Loading head, 2) Fixed support, 3) Sliding support, 4) Notch and groove (zoom on right figure) and 5) Inductive sensor. From [17].

2.4 Analysis of the results

The results are processed and analyzed in the same manner as in [3] to compare notched tests with non-notched tests. The study focuses on the following elements:

- The overall shape of the curve,
- The evolution of the stiffness of the specimen,
- The evolution of the residual notch opening,
- The shape of the imposed cycles.

For a complete analysis methodology, we invite the reader to refer to the details provided in [3]. However, we emphasize that the evolution of stiffness during loading can be obtained through an analysis of the slopes of the different cycles imposed during a test. It has been chosen, and justified in [3], to consider the measurement of the slope of the reloading path of a cycle to evaluate the structural stiffness of the bone, relative to the considered cycle. The evolution of stiffness is studied through the evolution of the relative stiffness reduction coefficient (W) defined in [3] as the relative difference in stiffness compared to the initial stiffness. Its expression is recalled below:

$$W = 1 - \frac{K}{K_0} \tag{1}$$

We also remind that the measurement of the residual notch opening is obtained for each cycle by extrapolating (linearly) to 0 the unloading path of the considered cycle.

Finally, the shape of the cycles is analyzed in relation to the evolution of their widths during the test. The width of a cycle is calculated as the quotient of its area by the amplitude of the imposed force [3].

3 Results

The raw results are expressed in terms of overall Force (P) versus Notch Opening (ω) curves, as shown in figure 2. Table 2 provides the maximum force values for each bone.

Figure 3 compiles the final crack paths for each conducted test. The views were captured using magnifying cameras (Dynolite USB microscopes) positioned on the lateral and medial sides of the bones. It is worth noting that, given the quasi-cylindrical shape of the bones, the cracking process initially localizes at the notch tip during the test and then propagates simultaneously in the lateral and medial portions before eventually converging towards the rough line. Although there are initially two cracks, lateral and medial, they are considered as a single cracking process, and the results are analyzed accordingly.

Table 2: Maximum forces reached for each specimen (NOD = notch opening displacement measured at the KAMAN KD 2300 inductive sensor.).

Reference	Max load [N]	NOD [mm]	Initial stiffness [N/mm]
150-17D	2591.2	0.40	10700
61-21G	2393.8	0.32	13127
90-21D	3848.7	0.30	17300
43-20G	2696.1	0.43	11070
80-21D	3400.6	0.37	15600

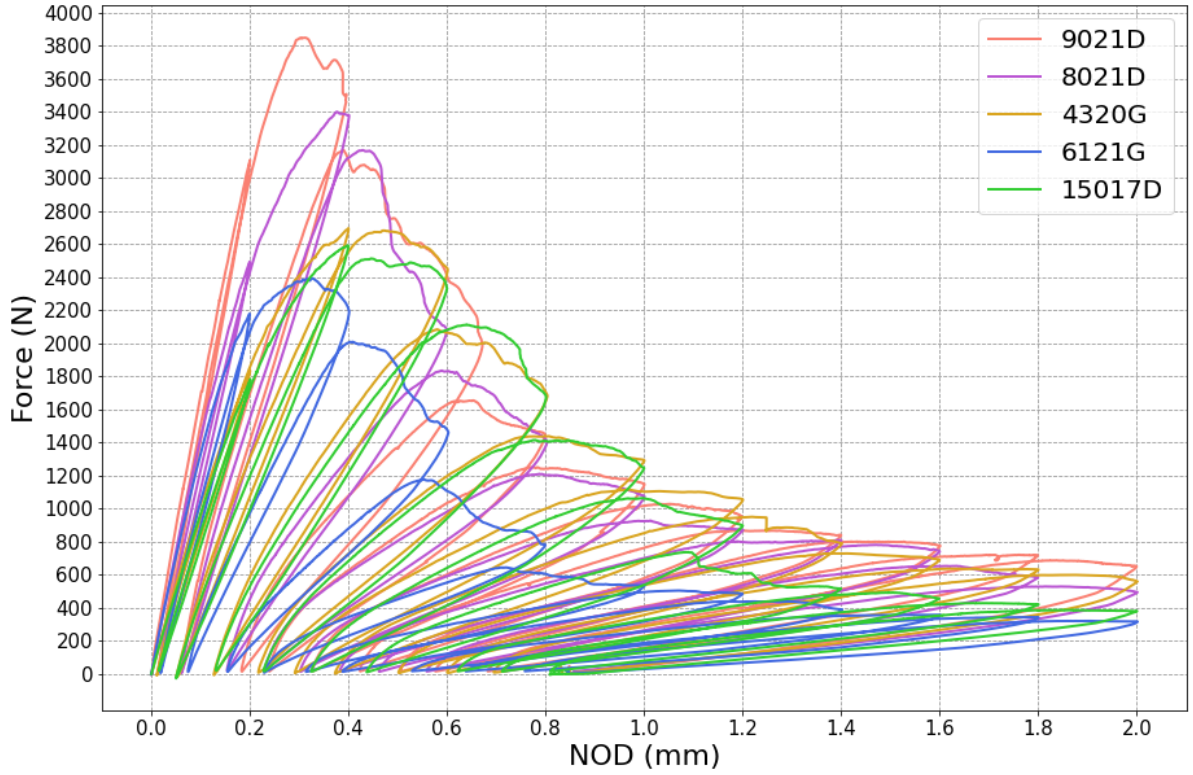

Figure 2: Crack propagation curves - Load vs NOD.

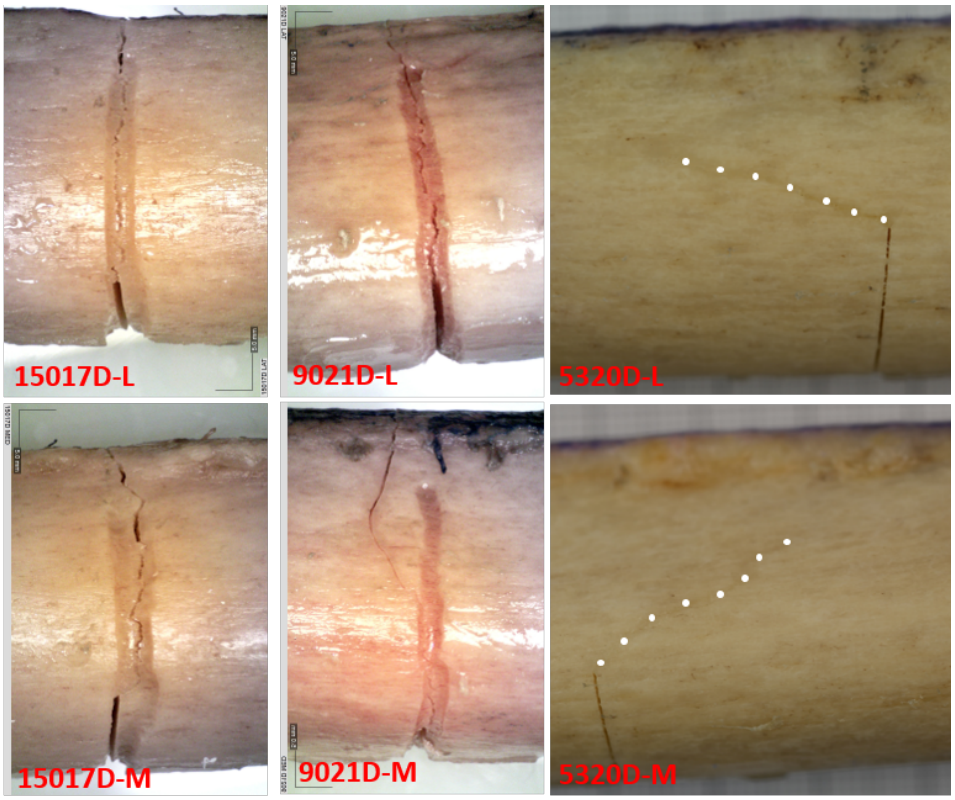

Figure 3: Crack propagation paths on each specimen. L and M correspond to the lateral and medial sides of the bone, respectively. The images of specimen 5320 are sourced from [3].

4 Discussion

4.1 Analysis of load vs notch opening (NOD) curves

The examination of the curves in figure 2 reveals that they all have similar shapes. Three phases can be distinguished:

- In their pre-peak regions, the obtained curves show evident nonlinearities. However, these are relatively weak from 0 to approximately 70% of the maximum force (see table 2). Subsequently, around 80 to 85% of the maximum force, these nonlinearities intensify more markedly, leading to the peak. These nonlinearities are indicative of physical processes corresponding to the formation of the Fracture Process Zone (FPZ) at the notch tip [5, 7, 12, 18, 19, 20], where stresses are concentrated. The literature has extensively detailed their potential origins, all related to phenomena affecting each scale of the material's microstructure [3]. We will mainly highlight that microcracks (in the range of 10 to 200 µm) appear at the notch tip, and this zone grows as the loading progresses.
- Around the loading peak, the densification and coalescence of these microcracks generate a macrocrack. At this stage, larger microstructural elements (porosity: Haversian and Volkmann canals, resorption cavity/interlamellar zone/cement lines, and osteonal structures) come into play and influence the crack propagation path [5, 8, 13, 20].
- In the post-peak region, the localized macrocrack propagates with its associated FPZ. The FPZ reaches its maximum size in this post-peak phase, sometimes slightly after the peak, and maintains a constant shape if not influenced by the proximity of boundary conditions. In this softening phase, the propagation of the macrocrack results in the gradual loss of load-bearing capacity of the bone [7, 19, 20].

In conclusion, two regimes can be considered in the cracking processes. In the pre-peak phase, these processes are dominated by the progressive diffusion of micro-damages (microcracking leading to material damage) at the notch tip. In the post-peak phase, they are dominated by the propagation of the macrocrack and its associated FPZ, leading to structural weakening.

It is also important to note that the observed dispersion in the overall curves, especially concerning their peaks and post-peaks, is related both to the different bone geometries and differences in internal microstructures [6, 10, 21].

4.2 Crack paths analysis

Figure 3 shows the macrocrack propagation paths obtained for different conducted tests (notched and non-notched). The best result on notched bone is in the case of specimen 15017D, where the macrocrack remains entirely confined within the notch. In other samples, the macrocrack exits the notch but still maintains a predominant orientation in the vertical direction (see sample 9021D in figure 3). No mechanism showing the influence of this exit from the groove is particularly visible on the experimental curves in figure 2. There is also no notable difference between the crack paths on the lateral and medial sides: the macrocrack can exit on either side, but it consistently tends to go slightly in the distal direction (towards the knee). This trend was already present in non-notched bones, where the crack consistently

propagated in this direction. It is also noteworthy that the crack exits the groove always after traveling a minimum distance of 5 to 10 mm inside the groove. In the case of non-notched tests (like sample 5320D in figure 3), the bifurcation of the macrocrack almost systematically occurred at the notch origin. The exit of the macrocrack is likely related to the fact that the notches may not be deep enough to sufficiently concentrate stresses and guide the crack. However, the choice of a depth of approximately 2 mm is a good compromise between providing sufficient action to keep the crack in a transverse orientation and having a minimal impact on the overall behavior of the bone.

4.3 Determination of the initial stiffnesses

As mentioned earlier, the overall curves in figure 2 start with a quasi-linear portion, and it is possible to calculate the slope of this section. The measurement of this slope provides the initial stiffness of the bone. The values obtained for each tested bone are indicated in table 2. The initial stiffness primarily depends on the microstructure and geometry of each specimen.

4.4 Evolution of the stiffnesses

Figure 4 represents the evolution of the stiffness reduction coefficient (W) as a function of the imposed notch opening in the considered cycle. The average value of W reached at the peaks of the tests is 0.36. It can also be observed that these curves reach their asymptote W=1 more quickly than that in [3]. This is clearly related to the presence of the notch, which forces transverse crack propagation and promotes a greater reduction in section than when the crack is deviated.

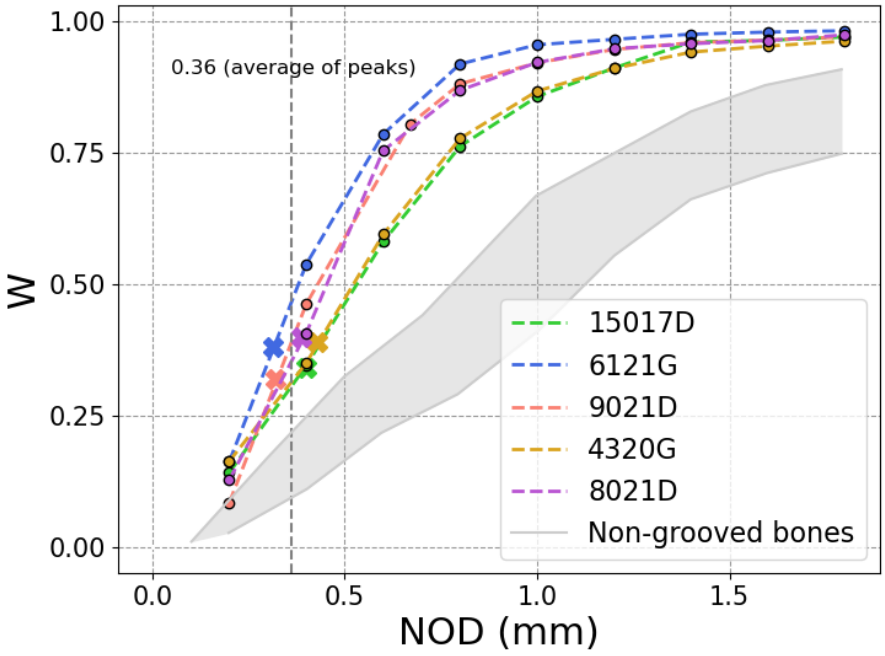

Figure 4: Decrease in the stiffness coefficient (W) as a function of the imposed cycle in NOD. The crosses represent the values at the loading peak for each bone. The gray zone corresponds to the overall envelope of similar curves from [3] for non-notched bones.

4.5 Evolution of the residual notch openings

The evolution of residual notch openings is plotted in figure 5 as a function of the imposed notch opening in the considered cycle. The curves show that nonlinear mechanisms lead to residual deformations after unloading. It should be noted that it has been demonstrated in [3] that these phenomena are visible for a notch opening of approximately 0.1 mm and negligible below that value. It is also noticeable that the results are relatively similar between the two types of tests (notched and non-notched). This indicates that the mechanisms inducing natural deformation are of the same nature and magnitude.

Figure 6 presents the evolution of residual notch opening as a function of W. Similarly to [3], the extrapolation to the origin of the curves indicates that residual notch openings are negligible for W=0. It is inferred that the cracking processes are the main cause of residual deformations. The observed differences with non-notched tests are primarily due to a different evolution of W for the two types of tests.

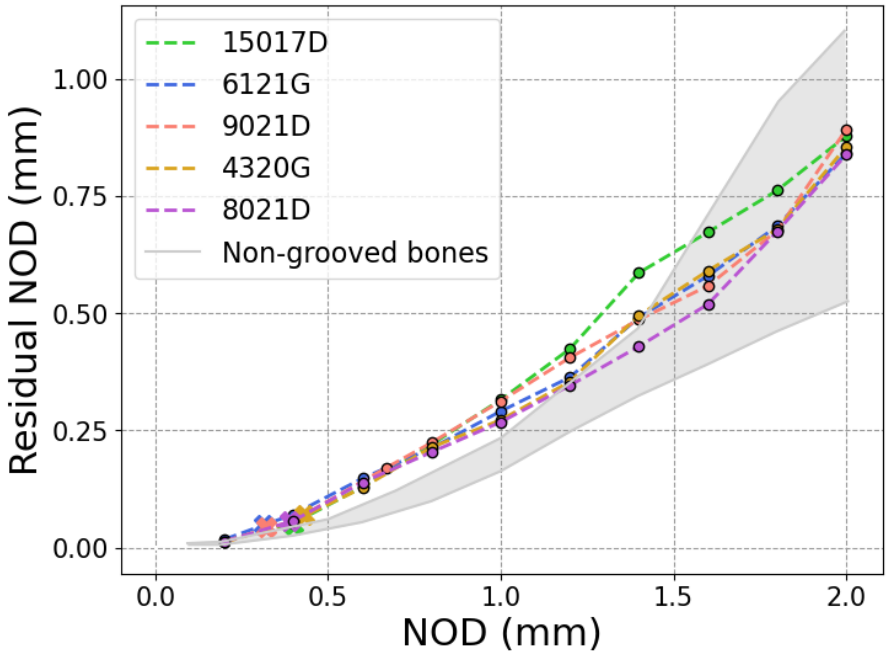

Figure 5: Evolution of the residual NOD as a function of the imposed cycle in NOD. The crosses represent the values at the loading peak for each bone. The gray zone corresponds to the overall envelope of similar curves from [3] for non-notched bones.

4.6 Cycle's shape

The unloading/reloading cycles exhibit a characteristic closed-loop shape. This particular form indicates the involvement of dissipative phenomena, primarily attributed to blockages related to crack interlocking and friction between the lips of the macrocrack and within the microcracks of the FPZ [22]. It is also noted that the reloading path does not pass through the unloading point that initiated the cycle.

Figure 7 shows the evolution of the cycle width as a function of the imposed notch opening in the considered cycle. It is observed that the obtained curves are very close to the envelope of those in [3], indicating similar mechanisms of the same magnitude.

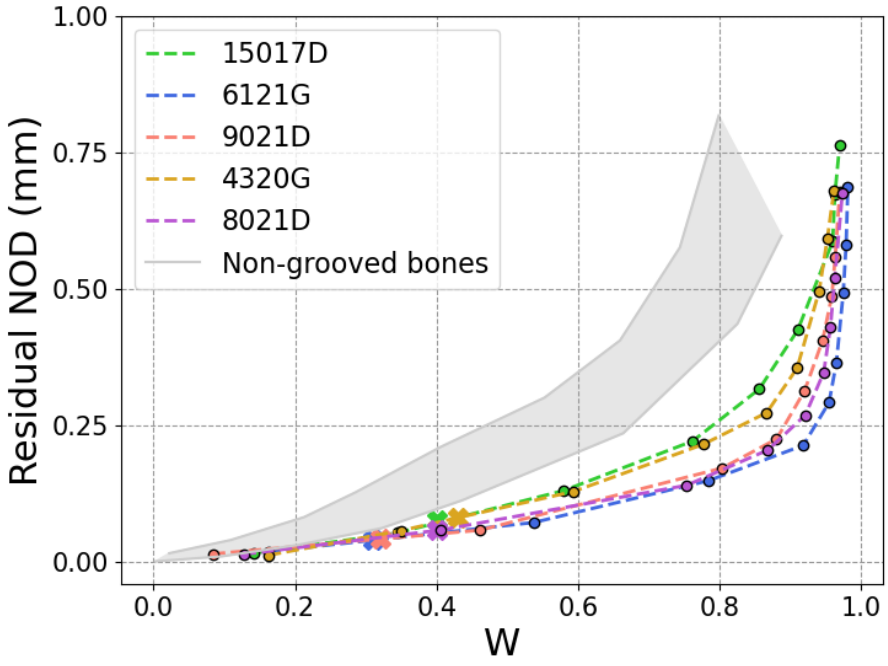

Figure 6: Evolution of the residual NOD as a function of the stiffness coefficient (W). The crosses represent the values at the loading peak for each bone. The gray zone corresponds to the overall envelope of similar curves from [3] for non-notched bones.

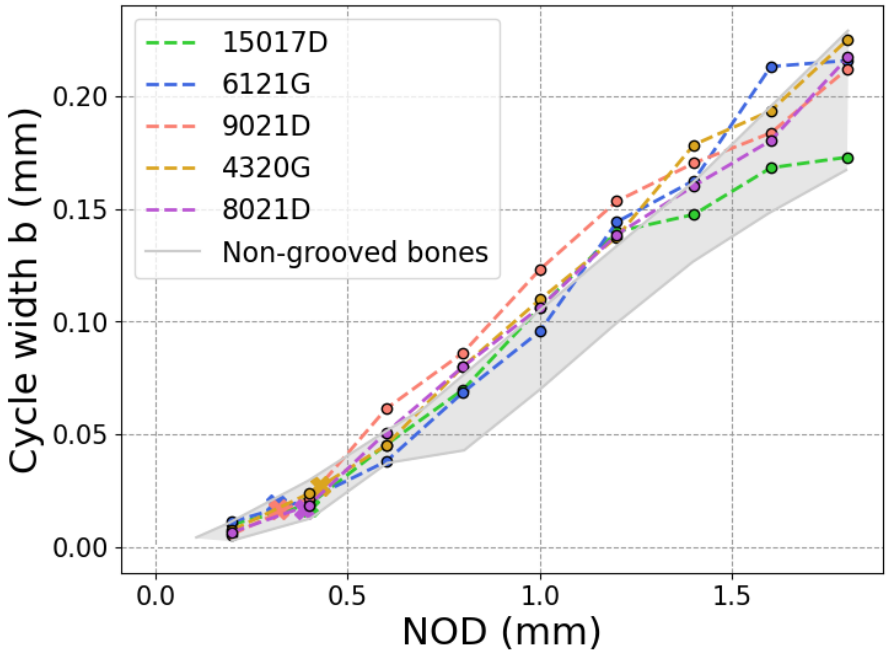

Figure 7: Cycle width as a function of the the imposed cycle in NOD. The crosses represent the values at the loading peak for each bone. The gray zone corresponds to the overall envelope of similar curves from [3] for non-notched bones.

4.7 Physical mechanisms

The obtained results are attributed to crack-related phenomena. Crack formation induces a progressive structural weakening (W increases, cf. figure 4) of the bone segments during loading. These phenomena

are also responsible for residual deformations, as there is a concurrent evolution of residual deformation with W (cf. figure 6). Furthermore, the results show that no plasticity is observable at this scale. While friction and blockage phenomena related to cracking may partially explain the residual deformations, they are not sufficient to fully account for the observed significant levels. Another mechanism (amplifier) operates simultaneously. It could involve a stress relaxation phenomenon during crack formation, preventing their complete closure during unloading and explaining a significant portion of the residual deformations. The existence of internal stresses in the bone tissue is explanable with the bone remodeling mechanism, as demonstrated in the literature [23, 24, 25]. This internal stress field is also highly heterogeneous, reflecting the nature of the material in which it developed. The release of internal stresses also helps explain the amplification of friction and interlocking phenomena influencing the shape of the cycles. It also explains why the reloading path of a cycle does not pass through the unloading point that initiated it (due to modifications in the cycle's stress field history during reloading).

5 Conclusion

A three-point bending mechanical test on a section of notched human bone is employed to investigate the propagation of a macrocrack in this type of tissue. The test is adapted to induce transverse crack propagation. The simplest guiding solution chosen involves creating a groove on the external lateral surface of the bone. The preparation of the specimen and its positioning on the machine received special attention to ensure a robust and repeatable experimental protocol. Unloading/reloading cycles show a decrease in the structural stiffness of the bone, a significant residual opening of the notch, and significant dissipative phenomena during the cycles. These observations are explained by the combined action of crack processes in a heterogeneous medium initially subjected to self-balanced internal stresses, a consequence of the bone remodeling mechanism. When a crack is created, it releases these stresses, locally disrupting the stress field (heterogeneous), preventing complete closure, and generating additional friction and amplified residual deformations. All the obtained results, in the form of relatively tight bundles of curves, show that the transverse guiding solution for the macrocrack, while not perfect, remains highly satisfactory.

It is also noteworthy that these tests will be subsequently used for the determination, through inverse analysis, of fracture mechanical properties in the transverse direction.

References

[1] T. Kurtz, Y. Godio-Raboutet, and J.-L. Tailhan. Propagation de fissure sur tronçon d'os long rainuré. 25ème congrès français de mécanique, nantes, france. *Association Française de Mécanique*, 2022.

[2] Y. Godio-Raboutet, T. Kurtz, C. Boulay, and J.-L. Tailhan. Crack propagation experiment on long human bone. *Computer Methods In Biomechanics And Biomedical Engineering*, 24:103–115, 2021.

[3] J.-L. Tailhan, T. Kurtz, Y. Godio-Raboutet, P. Rossi, and L. Thollon. Macrocrack propagation in a notched shaft segment of human long bone: Experimental results and mechanical aspects. *Journal of the Mechanical Behavior of Biomedical Materials*, 128:105132, 2022.

[4] J. C. Behiri and W. Bonfield. Orientation dependence of the fracture mechanics of cortical bone. *Journal of Biomechanics*, 22(8):863–872, 1989.

[5] Thomas Willett, David Josey, Rick Xing Ze Lu, Gagan Minhas, and John Montesano. The microdamage process zone during transverse cortical bone fracture: No ears at crack growth initiation. *Journal of the Mechanical Behavior of Biomedical Materials*, 74:371–382, 2017.

[6] Jae-Young Rho, Liisa Kuhn-Spearing, and Peter Zioupos. Mechanical properties and the hierarchical structure of bone. *Medical Engineering & Physics*, 20(2):92–102, 1998.

[7] J. C. Behiri and W. Bonfield. Fracture mechanics of bone—The effects of density, specimen thickness and crack velocity on longitudinal fracture. *Journal of Biomechanics*, 17(1):25–34, 1984.

[8] P. Zioupos and J. D. Currey. The extent of microcracking and the morphology of microcracks in damaged bone. *Journal of Materials Science*, 29(4):978–986, 1994.

[9] R. K. Nalla, J. J. Kruzic, and R. O. Ritchie. On the origin of the toughness of mineralized tissue: microcracking or crack bridging? *Bone*, 34(5):790–798, 2004.

[10] Mathilde Granke, Alexander J. Makowski, Sasidhar Uppuganti, and Jeffry S. Nyman. Prevalent role of porosity and osteonal area over mineralization heterogeneity in the fracture toughness of human cortical bone. *Journal of Biomechanics*, 49(13):2748–2755, 2016.

[11] J. B. Phelps, G. B. Hubbard, X. Wang, and C. M. Agrawal. Microstructural heterogeneity and the fracture toughness of bone. *Journal of Biomedical Materials Research*, 51(4):735–741, 2000.

[12] D. Vashishth, J. C. Behiri, and W. Bonfield. Crack growth resistance in cortical bone: Concept of microcrack toughening. *Journal of Biomechanics*, 30(8):763–769, 1997.

[13] Simin Li, Adel Abdel-Wahab, and Vadim V. Silberschmidt. Analysis of fracture processes in cortical bone tissue. *Engineering Fracture Mechanics*, 110:448–458, 2013.

[14] Peter Zioupos, Ulrich Hansen, and John D. Currey. Microcracking damage and the fracture process in relation to strain rate in human cortical bone tensile failure. *Journal of Biomechanics*, 41(14):2932–2939, 2008.

[15] Eugenio Giner, Ricardo Belda, Camila Arango, Ana Vercher-Martínez, José E. Tarancón, and F. Javier Fuenmayor. Calculation of the critical energy release rate Gc of the cement line in cortical bone combining experimental tests and finite element models. *Engineering Fracture Mechanics*, 184:168–182, 2017.

[16] J.J.L. Morais, M.F.S.F. de Moura, F.A.M. Pereira, J. Xavier, N. Dourado, M.I.R. Dias, and J.M.T. Azevedo. The double cantilever beam test applied to mode I fracture characterization of cortical bone tissue. *Journal of the Mechanical Behavior of Biomedical Materials*, 3(6):446–453, 2010.

[17] T. Kurtz, T. Woitrain, Y. Godio-Raboutet, F. L. B. Ribeiro, P.-J. Arnoux, and J.-L. Tailhan. Method for Evaluating Cortical Bone Young's Modulus: Numerical Twin Reconstruction, Finite Element Calculation, and Microstructure Analysis. *Journal of Biomechanical Engineering*, 145(111013), 2023.

[18] K. Piekarski. Fracture of Bone. *Journal of Applied Physics*, 41(1):215–223, 2003.

[19] W. Bonfield. Advances in the fracture mechanics of cortical bone. *Journal of Biomechanics*, 20(11-12):1071–1081, 1987.

[20] G. P. Parsamian and T. L. Norman. Diffuse damage accumulation in the fracture process zone of human cortical bone specimens and its influence on fracture toughness. *Journal of Materials Science. Materials in Medicine*, 12(9):779–783, 2001.

[21] R. Bruce Martin, David B. Burr, Neil A. Sharkey, and David P. Fyhrie. Fatigue and Fracture Resistance of Bone. In R. Bruce Martin, David B. Burr, Neil A. Sharkey, and David P. Fyhrie, editors, *Skeletal Tissue Mechanics*, pages 423–482. Springer, New York, NY, 2015.

[22] P. Acker, C. Boulay, and P. Rossi. On the importance of initial stresses in concrete and of the resulting mechanical effects. *Cement and Concrete Research*, 17(5):755–764, 1987.

[23] M. Tanaka, T. Adachi, and Y. Tomita. Bone remodeling considering residual stress: Preliminary experimental observation and theoretical model development. *WIT Transactions on Biomedicine and Health*, 1:1–8, 1970.

[24] Shigeru Tadano and Taro Okoshi. Residual stress in bone structure and tissue of rabbit's tibiofibula. *Bio-Medical Materials and Engineering*, 16(1):11–21, 2006.

[25] Dimitrios J. Hadjidakis and Ioannis I. Androulakis. Bone Remodeling. *Annals of the New York Academy of Sciences*, 1092(1):385–396, 2006.